Graphitic Edges and Unpaired π-Electron Spins

D. J. Klein* and L. Bytautas†

Texas A&M University at Galveston, Galveston, Texas 77553-1675

Received: February 10, 1999

The effects of different types of boundaries on graphite fragments are considered as they influence the π-electrons. From a simple resonance theoretic argument there are proposed simple structural conditions governing the occurrence of "unpaired" π-electron density near the edges. Predictions based on these rules are made for a variety of edge structures. Further, the novel resonance theoretic argument and predictions are strengthened through more elaborate considerations of both the valence bond and molecular orbital theoretic nature, especially for translationally symmetric polymer strips with various types of edges.

1. Introduction

Graphite and the behavior of the π-electrons therein has long been of interest. Most of the theoretical work has focused on the bulk properties. Within the simple Hückel molecular orbital (MO) framework, solutions[1,2] for the π-electron bands of extended systems go back about 5 decades, with hundreds of more recent articles. On the other hand more successful quantitative work within a resonating valence bond (VB) framework for such extended systems is more recent, perhaps starting a decade back,[3] but now with very much work as reviewed in ref 4. And the whole area of conjugated π-networks is of continuing intense interest, especially with the advent of fullerenes and "buckytubes", and the possibilities[5] of related nanostructural devices.

Real graphite has boundaries or edges, and often markedly so, in the sense that most graphite is rather impure, consisting of smaller pieces or having rather many imperfections that may often be viewed to introduce an additional (internal) boundary edge. Experimentally occurring graphites seem typically to be ill-characterized in terms of the nature of the edges or of the imperfections and instead often seem to be characterized[6,7] in terms of a few bulk properties and methods of preparation. Thus, theoretical work on the effect of different graphitic boundary structures on the behavior of the π-electrons may be especially valuable, particularly if simple rules can be discerned. Further, such work should also be of much use for the characterization of carbon nanostructures.[5]

Here, simple rules concerning the effect of different types of edge structures on the π-electrons are sought. As so thoroughly illustrated by Pauling,[8] resonance theory offers a ready method to qualitatively treat many molecular species, and in the approach to be taken in section 2 here, a modified simple version of this resonance theoretic view is used. From this approach a simple method emerges to correlate molecular and electronic structure at graphitic edges. The resultant rules stated in section 3 are quite simple, though they do not seem to have previously been so fully articulated. The application of the rules to a number of particular cases is illustrated, and they are also noted to make some rather general predictions concerning unpaired spin densities for different translationally symmetric edges on graphite. These simple rules of section 3 may be applied without reference to any other sections concerning their theoretical justification.

The simple resonance theoretic based picture is elaborated in more theoretical detail in sections 4 (from a VB viewpoint) and 5 (from an MO viewpoint). Basically, with closer attention to Kekule structures, section 4 provides deeper VB theoretic evidence, following some earlier work;[9] that is, a more detailed foundation is pursued for the implicitly averaged effects of Kekule structures utilized in the picture of section 2. But the VB theoretic approach contrasts with the conventional quantum chemical approach for the treatment of molecular structures, including edges or surfaces, such being by way of MO or band theory. For example, in reviews 10 and 11 concerning the electronic structure at surfaces or in the particular cases studied in refs 12−14 on the characterization of the electronic structure of graphitic edges, there is no mention of resonance theory or VB theory. Now with such alternative MO theoretic schemes, systems are usually treated on a case-by-case computational manner so that rules emerging from it would be more or less empirical, with the MO computations playing the part of (computer) experiments. Section 5 considers some theoretical and computational evidence from a simple Hückel MO theoretic framework, with these arguments being brought to a reasonable conclusion only through the inclusion of electron−electron interactions, most simply using an unrestricted Hartree−Fock solution to a Hubbard−PPP model. Such computed MO band theoretic results[12−16] turn out in the cases so far investigated to be in close agreement with the simple resonance theoretic picture, and there is a degree of agreement with some other particular MO computations[17−19] on large benzenoids. A number of band theoretical results consistent with the resonance theoretic picture are also established in a general manner in which the unpaired electrons appear in this alternative approach emerging (and explaining a number of earlier special case observations). Overall, the simple rules of section 3 seem to be generally supported via both VB and MO theoretic evidence.

Throughout the present considerations the σ-network is considered only insofar as providing a frame in which the π-electrons are to move. Of course, with edges there are σ-electrons on the edge also and if allowed to "dangle" could conceivably contribute to a reconstruction of the edge to a "nonclassical" structure. Here, it is imagined that no such

† On leave of absence from Institute of Theoretical Physics and Astronomy, Gostauto 12, 2600 Vilnius, Lithuania.

10.1021/jp990510j CCC: $18.00
Published on Web 06/15/1999

reconstruction occurs so that the structure of the network up to the edge is just a subsection of an infinite graphite sheet. That is, the structures presently presumed are to be just that of subsections of the honeycomb lattice. One might imagine the σ-electrons from the carbons at the edges to be bonded to some terminating atoms such as H atoms. If bonded to O atoms or OH groups, there are of course additional π-electrons to take into account, but this is to be left for future consideration, though it is surmised that similar ideas can apply. Indeed, resonance theoretic ideas should presumably be of interest in a more general materials science context, for though Pauling's work in a qualitative mode on finite molecules seems well accepted in some quarters, comparatively less use seems to be accepted as successful in treating extended solid-state or polymeric systems.

2. Resonance Theory for Graphitic Edges

Conventional qualitative resonance theory[8,9,20,21] is based on the consideration of sets of different classical chemical bonding patterns consistent with the given structure. Further, the greater the number of such low-energy VB patterns the greater the stabilization (because of configuration interaction among them). And of course an individual VB bonding pattern is lower in energy the greater the number of neighboring singlet spin-paired bonds there are. Thus, there are two tendencies competing to maximize overall energetic stability: maximization of the number of neighbor-paired sites and maximization of the number of resonance structures. Thus, since the edge is such a small fraction of the bulk (if the graphitic fragments are large), one might allow nonneighbor-paired sites confined to the region of the edges if this circumstance notably enhances the number of VB bonding patterns. That is, resonance stabilization in the N atom bulk might overcome the loss of these relatively few $\sim N^{1/2}$ unpaired π-electrons near the edge. [At least for "ordinary" shaped fragments, the boundary should have $\sim N^{1/2}$ atoms.]

Thus, the argument devolves to the consideration of classes of VB bonding patterns with satisfaction of the first rule above, indicating that any nonneighbor-paired sites should be confined to the edge region. Then in consequence of the second rule above, such classes having the greatest numbers of members are sought. But in fact the characterization of the class with the most numerous Kekule bonding patterns is somewhat intuitively clear; resonance should be greatest when the bonding patterns are as delocalized as possible. That is, one might anticipate (and correctly so, as elaborated in the section 4) that in the bulk region the probability of a double bond along any one of the three directions away from a site to its nearest neighbors is equally likely. This probability is essentially a bond order as often defined[22] in treating benzenoids; the *Pauling bond order* for a given bond of a conjugated hydrocarbon is just the fraction of the (fully paired) Kekule structures for which the given bond is double. Thus, the preferred classes of VB bonding patterns for large graphitic fragments should be those such that the π-bond orders are very close to $^1/_3$ in the bulk of the fragment.

But now there are notable consequences if the π-bond orders are close to $^1/_3$ in the bulk and if any deficit of the sum of the bond orders at any site near the edge represents nonneighbor-paired electron density. This deficit might be termed a *residual free valence*. Thus, near the edge one can identify as in Figure 1 different local arrangements for bond orders if the connections toward the interior have a bond order of $^1/_3$. Here, edge bonds are allowed to have values differing from $^1/_3$ if it leads to a more complete saturation of the free valence, remnant nonzero values of which are indicated in small circles marking the

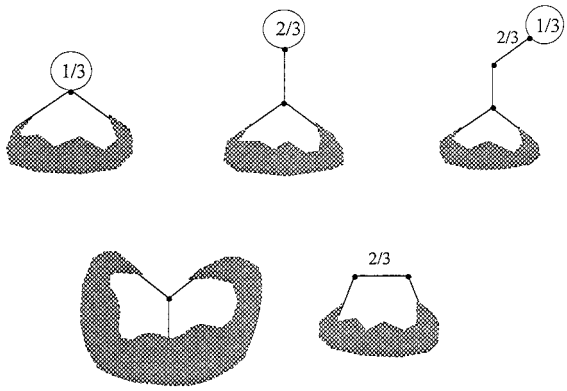

Figure 1. Different possible local types of graphitic boundary structures, along with any presumed (zero-order) π-bond orders differing from $^1/_3$ and residual (zero-order) free valences, which are encircled.

associated sites. Thus, it is seen that different types of edge structures lead to different amounts of free valence at the edges.

A further refinement concerns the range of any pairing between nonneighbor sites. If the distance between two nonneighbor sites is smaller, then such a pattern being more similar to a preferred neighbor-pairing pattern is more stabilizing than a pattern with free valences, which are necessarily very distant. But in the implementation of these ideas, it is important to note the following: first, that the graphite lattice is *bipartite* in the sense that[23] it can be divided into two subsets (usually called *starred* and *unstarred*) such that any site from one subset has its neighbors solely in the other subset; and second, that the singlet spin pairing is[24] preferred solely between sites in different subsets. Free valences on a boundary can then be (partly) satiated by nearby free valences only if they are located on different types of sites (i.e., starred vs unstarred sites). That is, the free valences on the starred and unstarred sites might be identified with "+" and "−" signed *spin densities*, with spin pairing only between oppositely signed spin densities, with the strength of the pairing diminishing with separation. Thus, for the different kinds of regular (i.e., translationally symmetric) edges appearing in Figure 2, there is pairing between either nearest neighbors or next-next-nearest neighbors so that these edges are not so reactive, most especially that in Figure 2a. Likewise, for the different types of regular edges in Figure 3 there is pairing possible only to some distant sites, say on an opposite edge, so that these edges (being presumed distant) are reactive and exhibit essentially unpaired spin density localized along the edges of the fragment; that is, these edges are *polyradicaloid*. Moreover, these ideas apply to characterize many other types of edges. And the overall argument may be expressed as a simple set of rules presented (and applied in the next section).

3. Local Unpaired Spin Density: Rules, Application, and Discussion

The discussion of the preceding section leads to simple rules for edge-localized spin density. For the special case of translationally symmetric edges there are especially simple purely structural rules, where details of the underlying resonance theoretic picture have been refined away, as in eq 3.2, but first a set of slightly more general rules with attention to the zero-order resonance theoretic picture and with wider applicability are given. From the preceding discussion the following are the simple rules.

(a) Assign π-bond orders of $^1/_3$ to each edge issuing from a site of degree 3.

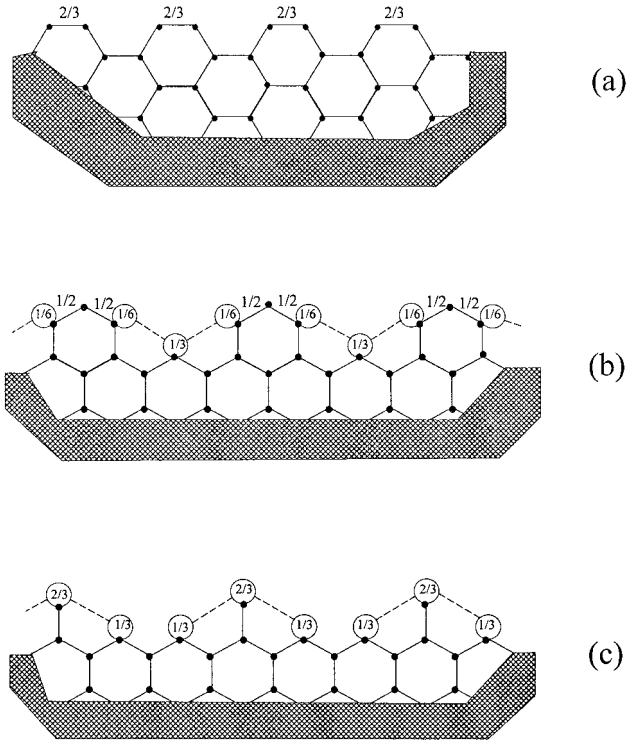

Figure 2. Portions of different types of translationally symmetric graphitic edges giving rise to no net spin density at the edges. The zero-order non-$^1/_3$ bond orders at the edges are indicated, as also are the associated zero-order free valences, which for the cases shown can be paired between nonneighbor starred and unstarred sites as indicated by dotted lines.

(b) Assign the remaining π-bond orders to be as large as possible subject to the constraint that the sum of the π-bond orders of no site exceeds 1.

(c) Calculate zero-order free valences v_i at each site i as the deficit from 1 of the sum of the π-bond orders p_e incident at that site (i.e., $v_i = 1 - \sum_{e\sim i} p_e$).

(d) The unpaired spin density at an edge is the difference between the net free valence of starred and unstarred sites nearby on an edge.

Again, a refinement of the last two rules would take more explicit account for pairing between next-next-nearest neighbors (or perhaps even a little more distant), thereby identifying generally more accurately the unpaired spin density and its location.

As these rules stand they are rather simple to apply, which we have done for the edges of Figures 2−4. The more comprehensive listing of Figure 4 identifies just a unit cell of edge (where the structures of the more extended representations of Figures 2 and 3 are repeated). These unit cells are conveniently labeled by the primitive translations along the edge direction, such a label being a two-digit code (x,y) with x identifying the number of hexagon center to neighbor hexagon center steps along one direction imagined to be from left to right and y identifying the number of similar steps along a second direction rotated 60° counterclockwise. It is a matter of convention to choose

$$0 < x \geq y \geq 0 \qquad (3.1)$$

These associated translation symmetry labels and the consequent predicted numbers $\#_u$ of unpaired electrons per unit cell of edge as pictured in Figure 4 are reported in Table 1. And the last column of the table is discussed in section 5. It is seen from the table that thrice the number of unpaired electrons per unit cell is always an integer.

The resultant predictions for such translationally symmetric edges can be given an even simpler purely structural presentation. Rule d uses the phrase "nearby", which for the case of translational symmetry can be given a quite precise formal meaning in terms of sites within the same unit cell of edge. Further, for the net spin density, the precise locality of the unpaired spins does not matter, so one might use just a zero-order picture with a bond order of $^1/_3$ (initially) assigned to every bond, and the corresponding zero-order free valences are 0, $^1/_3$, $^2/_3$, or 1 for sites of degree $d = 3$, 2, 1, or 0, though of course we still need to pay attention to further pairing between opposite types of sites. The results can be neatly expressed in terms of the numbers $\#_{\star d}$ and $\#_{od}$ of starred and unstarred sites of degree d per unit cell, where the number $\#_u$ of unpaired electrons per unit cell of edge is seen to be predicted to be

$$\#_u = \left|\left\{\frac{2}{3}\#_{\star 1} + \frac{1}{3}\#_{\star 2}\right\} - \left\{\frac{2}{3}\#_{o1} + \frac{1}{3}\#_{o2}\right\}\right| \qquad (3.2)$$

which is a purely structural condition. There is a further result that allows one to exclude many symmetry classes of edges from ever being nonradical, namely, the symmetry−integrality theorem: Within the simple resonance theoretic picture as applied to translationally symmetric edges of symmetry class (x,y), the number $\#_u$ of unpaired electrons per unit cell is an integer if and only if $x - y$ is a multiple of 3. A proof is given in Appendix A. Stable (nonradical) translationally symmetric edges can occur only among those of symmetry classes (x,y) with $x - y$ divisible by 3.

For the polyradicaloid case the unpaired spin densities are not necessarily so severely localized as one might surmise from such rules (as illustrated in Figure 3). That is, one can imagine the free valences locally moved around to other nearby atoms, say as done in Figure 5. But the free valence on a particular type (starred or unstarred) of site is conserved (as is more or less empirically evident but which is also shown in section 3), and the farther the free valences are moved the greater the region where there is less maximally resonant bulk material with π-bond orders of $^1/_3$ in each direction. That is, the net unpaired spin densities are not completely localized but tend to stick near the boundary to the same types of sites. But rearranging the bond orders and allowing the free valences to be more smeared out still gives rise to the same numbers of unpaired electrons near the edge. That is, without even explicit construction of Kekule structures predictions are readily reached as to the extent of unpaired electrons showing up on a given type of graphitic edge, and some indication is obtained of where it shows up.

Of course, sites with higher residual free valences should be more reactive. That is, if an edge forms with higher free valence values, then one can anticipate that the edge is reactive, preferably forming, say through addition reactions, new local structures that exhibit less free valence. Therefore, there are implications as to the types of stabilized edges as could appear on large graphite fragments. Also, unpaired electrons at the edges should enhance a material's paramagnetism, which is in fact observed for some graphites, with some graphitic materials showing[7] exceptional paramagnetism perhaps because of unusual edge structures. Further, there should be implications for regular conjugated hydrocarbon polymer strips, several simpler types of which have received much experimental treatment over the last couple of decades, notably polyacetylene[25] and poly-*p*-phenylene.[26] Indeed, similar ideas apply to correlating locally unpaired spin densities at the ends of polymer strips with the

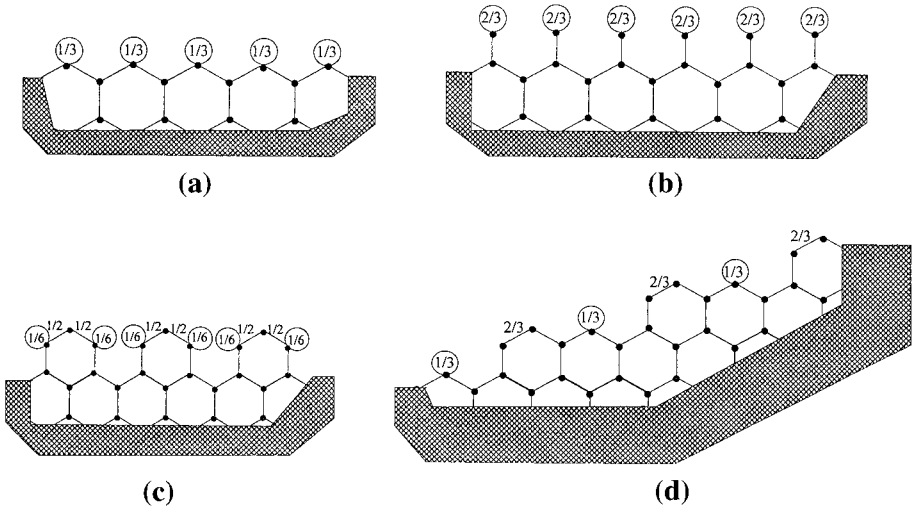

Figure 3. Portions of different types of translationally symmetric graphitic edges giving rise to nonzero net spin density at the edges. The zero-order non-$^1/_3$ bond orders at the edges are indicated, as also are the associated zero-order free valences, which here (being on like type sites) remain unpaired.

type of strip structure and the various end structures, but this we do not pursue here, it having already been done[3,27] in the more elaborated format of section 4.

4. Resonating VB Theoretic Refinement

Notably much of the resonance theoretic argument of the preceding section can be made a little more complete, following more traditional resonating VB theoretic lines with a more explicit consideration of "Kekule structures", such as already considered somewhat in ref 8. Often *Kekule structures* are viewed[28] to be VB bonding patterns wherein every site is paired to a unique neighbor. But in order to treat radicaloid systems, this constraint is relaxed for the condition that there be a maximal pairing of neighbors (where some may be left unpaired as when there are an excess of starred sites over unstarred sites). Here, we term maximally paired bonding patterns *global* Kekule structures and utilize even more weakly constrained *bulk* Kekule structures, which are to have all sites neighbor-paired except perhaps some few at the edges. It is the distinction between these global and bulk structures that is crucial in the present context. Now one naturally anticipates that Kekule structure counts should be *multiplicative* in the sense that for the case of two disconnected fragments A and B each with counts K_A and K_B the overall count is $K_{AB} = K_A K_B$, so especially for a large N site system G with count K_G it is appropriate to deal with the Kekule structure count per site defined as

$$\kappa \equiv K_G^{\,1/N} \tag{4.1}$$

And whether nonneighbor-paired spins near an edge occur then is a question that involves the consideration of the bulk values for κ. In particular, it is to be considered how κ depends on the type of edge if all sites are required to be neighbor-paired (as in a global Kekule structure) and how this deviates from the maximum value of κ otherwise attainable allowing only a few unpaired sites near the edge.

That such different bulk values of κ are possible has to do with a long-range order that occurs for Kekule structures and that can be characterized in terms of a "cut" that divides the molecular π-network graph G in two. A *cut* is a subset C of neighbor pairs of sites of G such that if the bonds of the site pairs of C are deleted from G, then the graph falls into two disconnected pieces, say A and B. Further, given a cut C, there is an associated *cut partitioning* into two subsets $C_\star$ and $C_\circ$, since the A end of a neighbor pair of C is starred or unstarred. An example of a cut C on pyrene is indicated by the dotted line in Figure 6; i.e., the bonds intersected by the dotted line are those in C. The associated cut partitioning of C is $C_\star \oplus C_\circ = \{\{1,2\}\} \oplus \{\{5,6\},\{11,10\}\}$. Note that the net partitioning of C is independent; the first of which set of sites are called starred or unstarred; and second of which the subgraph is taken as A or B (though what is called $C_\star$ and $C_\circ$ might be interchanged). A given (global) Kekule structure K may be thought of as a certain subset of graph edges, some of which may be common to a given cut C, and one may define a particular characteristic

$$\Delta(C,K) \equiv ||(K \cap C_\star)| - |(K \cap C_\circ)|| \tag{4.2}$$

That is, $\Delta(C,K)$ can be described as the difference in numbers of π-bonds of K identified as neighbor pairs of $C_\star$ and of $C_\circ$. A cut C for the case of phenanthrene is in Figure 7, indicated as a dotted line in each of the five (global) Kekule structures. In this case one of the two sets $C_\star$ or $C_\circ$ is empty and the difference between their orders is ± 1 (for every Kekule structure). Now the Kekule structure invariants of interest may be characterized in a theorematic form as the pairing conservation theorem: Let G be a bipartite graph with a cut C and a cut partitioning into $C_\star$ and $C_\circ$. Then every global Kekule structure of G has the same difference $\Delta(C)$ in numbers of π-bonds identified as neighbor pairs of $C_\star$ and of $C_\circ$.

This theorem, which asserts K independence of $\Delta(C,K) = \Delta(C)$, is proved in the Appendix B. That is, despite the seeming disorder of π-bond arrangement among the different global Kekule structures, there is something that is "conserved", and conservation principles typically have important consequences.

The relevance of this cut invariant is illustrated for a polymer strip as in Figure 8 where there is identified a (translationally equivalent) sequence of local cuts C_{loc} each marking a boundary of a unit cell. Since each such local cut is (translationally) equivalent, one might expect that the $\Delta(C_{loc})$ at every boundary should be the same, and this indeed is the case, as is illustrated for two Kekule structures also shown in Figure 8. But the two different Kekule structures shown have different values for $\Delta(C_{loc})$, as can be consistent with the theorem only in the following certain circumstances: if the Kekule structures are

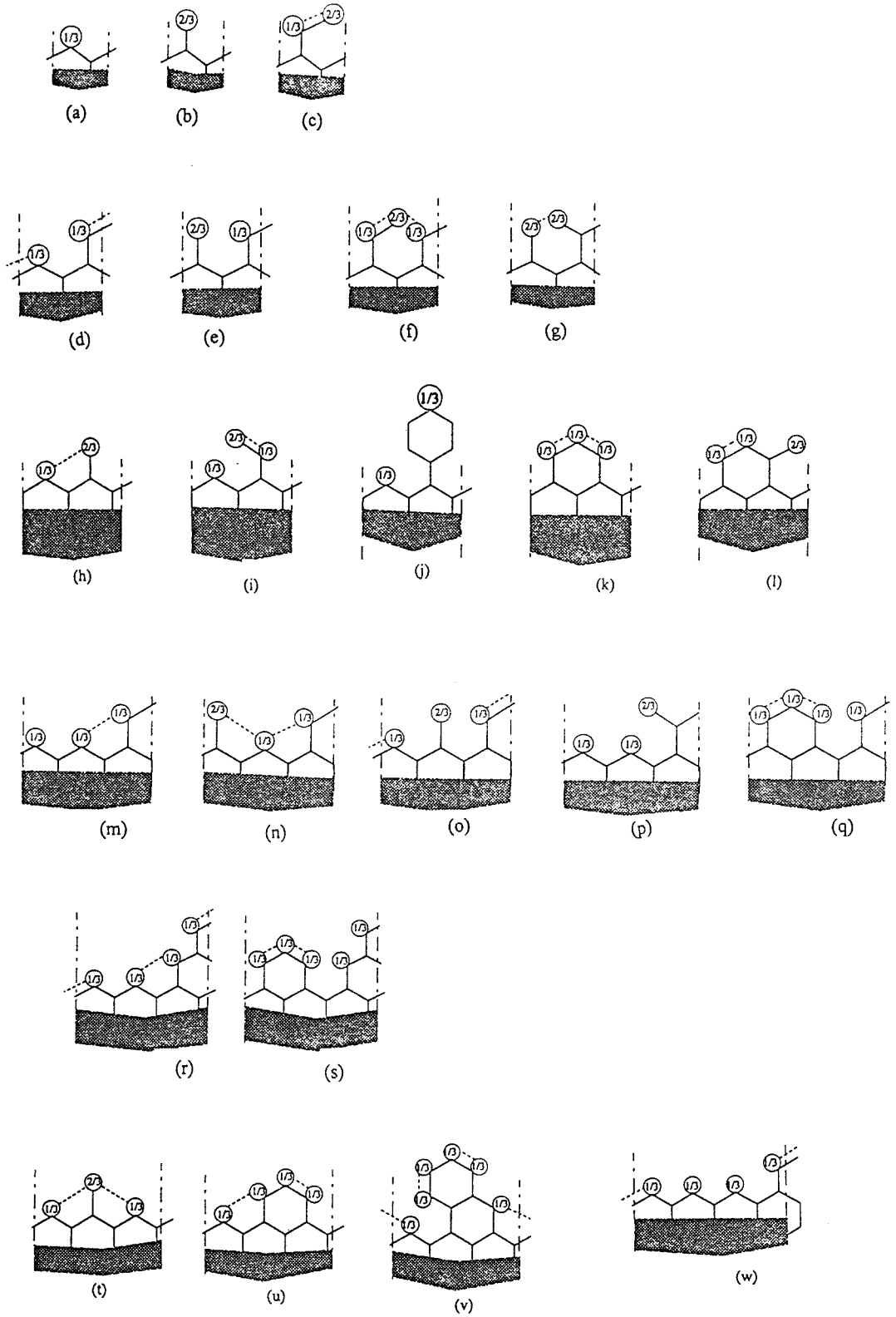

Figure 4. Unit cell portions of various possible graphitic edges, with the vertical dashed lines indicating the boundaries of the unit cells. Nonneighbor pairing between sites unpaired in zero-order is indicated with (nonvertical) dashed lines.

not global and at least one has some unpaired sites at the ends of the polymer chain; if the two Kekule structures are global, they occur on two polymer chains differing slightly in their end structures; if the polymer has cyclic boundary conditions, where it takes two of the unit cell boundaries to make a complete cut C_{com} consisting of two local cuts so that the two global Kekule structures end up having the same $\Delta(C_{com})$ (=0 if the two local cuts are translationally related).

Indeed, in the earlier treatment[29] developing some aspects of the present theorem, the system (though not necessarily translationally symmetric) was imagined to be embedded within the "dough" of a doughnut (i.e., a solid torus) such that linked sites were spatially close, and a cut was local so as not to disconnect the doughnut; all this avoided any discussion of our bulk Kekule structures or edges, as made convenient the consideration of the bulk consequences of the ordering. In any event with the

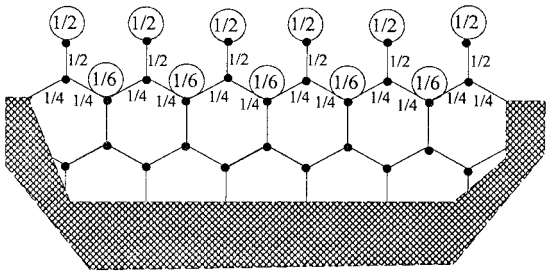

Figure 5. Modified assignment of bond orders for the same boundary as in Figure 3b. Note, however, that the same amount of residual free valence (on the same type of sites) remains.

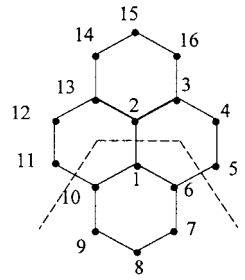

Figure 6. Example cut C on pyrene.

consideration of bulk Kekule structures one can still define a local difference $\Delta(C_{loc})$ though now different values are possible, but structures K with different values of $\Delta(C_{loc})$ differ everywhere in the bulk of the material and so must be essentially noninteracting (as long as interactions are local). Thus, the bulk Kekule structures fall into different *resonance classes* associated with different values of $\Delta(C_{loc})$. Because of the lack of interaction between bulk Kekule structures of different resonance classes, there is a separate ground state associated with each such class. These different resonance classes each have their own Kekule structure count κ per site so that often one will have (exponentially) more structures and be preferred (in giving rise to a lower energy, more resonant ground state) even if this leads to unpaired electrons at the polymer strip ends. Moreover, these considerations lead rather directly to interesting possibilities for solitonic excitations, as discussed elsewhere.[27]

A crucial point of consideration in the argument of the preceding section is the manner of dependence of the resonance energy on the number of Kekule structures and in particular on κ. Given a Kekule structure, its interaction with others (i.e., its resonance) is governed by the number of ways of making a small local modification to change it to another Kekule structure. One such local change is an alternation of the pattern of bonding around a conjugated six-circuit (this being a hexagonal ring with alternating single and double bonds), as illustrated in Figure 9. Evidently, resonance energy should involve an average over all Kekule structures (within one resonance class) of the number of such local patterns of modification. Indeed, the so-called "conjugated circuits" model[30] is formulated to manifest this quite explicitly. But the usual Pauling−Wheland resonance theoretic VB model on the basis of Kekule structures manifests this class-confined interaction,[3,9,27] just with a more involved sort of averaging. For typical highly resonant Kekule structures, this average number of possible local modifications should scale with the number N of sites, and indeed, this clearly is a bound for the rapidity of scaling. Now also this average number ($\sim N$) of such local modifications to yield new Kekule structures should be qualitatively related to the number κ of Kekule structures per site. Indeed, if one imagines that the number of local changes that can be made independently also is of the form $\sim cN$, then the number of Kekule structures that may be made from a typical Kekule structure is $\sim 2^{cN}$, since one either makes or does not make the change in each of the $\sim cN$ independent positions. But also the number of Kekule structures must be bound by $\sim 3^{N/2}$ (where we imagine that each of the $\sim N/2$ starred site has no more than three choices for which the unstarred site is to be paired to in a Kekule structure). Thus, the number of Kekule structures for the more highly resonant Kekule structure classes should scale as κ^N with $\kappa > 1$ and typically with a greater value for κ the greater the resonance energy per site. Indeed, this is quantitatively shown[3] as a function of resonance class for a sequence of strips. Typically, $\log \kappa$ should be roughly proportional to the resonance energy per site, and in particular, the resonance classes with larger κ should be more stable (i.e., have higher resonance energy).

Another crucial consideration in the argument of the preceding section is that pairing is dominated by that between sites of different types (starred or unstarred), with nearer such pairings giving rise to greater stabilization and larger exchange-mediated splittings among states of different spin multiplicities. First, very distant singlet spin pairings act much the same as triplet pairings or no pairings. That is, if distant singlet spin pairings in a wave function are replaced by triplet pairings, there is little effect on the energy, since the coupling to anything with nearby pairings instead is very weak; either the direct interaction in the Hamiltonian H_{VB} is very small or it takes many applications of neighbor exchange interactions in H_{VB} to bring the pairing to nearby sites. Thus, pairings from one side of a wide strip to the other may be neglected and the spins so involved may be effectively viewed as unpaired. Indeed, for such unpaired spins on a wide strip, one may expect them to act just as a modified strip would with the far side of the strip having no locally unpaired spins.

Some aspects of the present argument are identifiable in earlier work. A notable part of the present discussion is found in ref 27, but also some other aspects are found elsewhere without recognition of their relevance. For example, Yen,[31] Gordon, and Davison,[32] Elser,[33] and Stein and Brown[17] with different special boundaries find Kekule structure counts per site that are smaller than the "proper" bulk value found when there are either no boundaries (i.e., cyclic boundary conditions) as in ref 34 or suitable boundaries (as that in Figure 2a).[27] That is, refs 17 and 31−33 in essence count what we have termed global Kekule structures associated with nonmaximally resonant resonance classes, whereas the different counts of ref 34 are for all classes (which asymptotically are essentially the maximally resonant resonance classes).

Finally, there is a kind of check on the preceding arguments, since for a molecule it leads to a prediction of the global spin symmetry, which may be compared to more exacting results. That is, taking into account spin pairings regardless of their range, the number $\#_{un}$ of unpaired electrons for a molecule as a whole may be calculated in terms of the zero-order free valences for the different types of sites. Then the relation of eq 3.2 still holds if $\#_u$, $\#_{\star d}$, and $\#_{od}$ denote the numbers per unit cell rather than per molecule (or alternatively, we might view the molecule as a whole as consisting of just one unit cell). Now recalling that every bond has one starred and one unstarred end, counting bonds can be done in two ways: by counting the dangling bonds out of starred sites (thereby giving $\#_{\star 1} + 2\#_{\star 2} + 3\#_{\star 3}$) and by counting the number of dangling bonds out of unstarred sites (thereby giving $\#_{o1} + 2\#_{o2} + 3\#_{o3}$). Thus,

$$\#_{\star 1} + 2\#_{\star 2} + 3\#_{\star 3} = \#_{o1} + 2\#_{o2} + 3\#_{o3} \qquad (4.3)$$

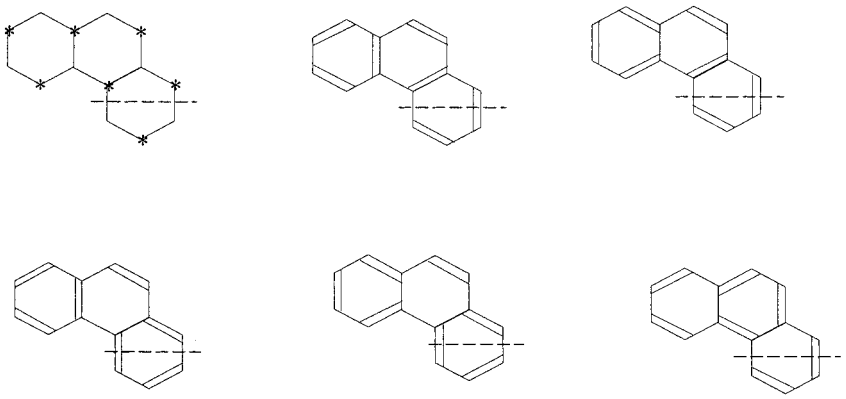

Figure 7. Phenanthrene cut with partitioning $C_\star \oplus C_\circ$ and the five associated Kekule structures.

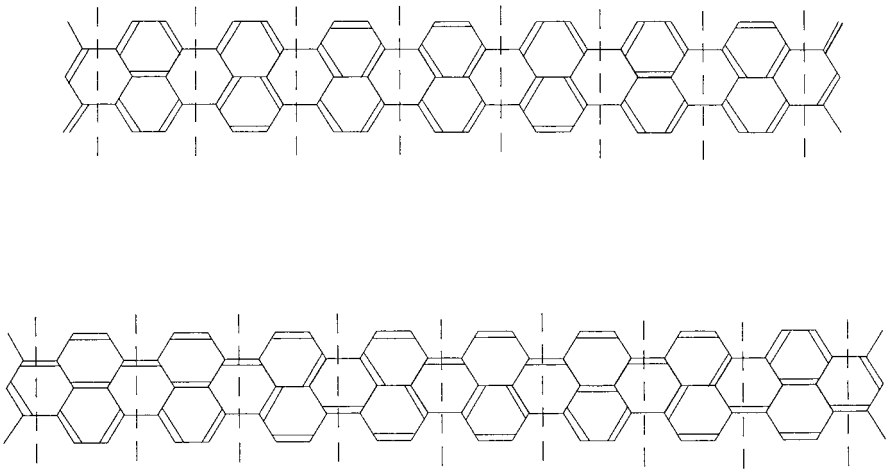

Figure 8. Polymer strip with Kekule structures each with a different number (0 and 1) of π-bonds crossing every unit cell boundary (and therefore in two different resonance classes).

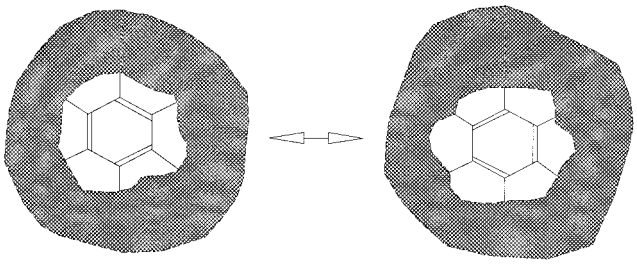

Figure 9. Two Kekule structures locally differing only at a single hexagon in the interior.

and of course, the total number of starred and unstarred sites are respectively given as

$$\#_\star = \#_{\star 1} + \#_{\star 2} + \#_{\star 3} \quad \text{and} \quad \#_o = \#_{o1} + \#_{o2} + \#_{o3} \quad (4.4)$$

Then using relations 4.3 and 4.4, one may reexpress eq 3.2 as the number of globally unpaired spins in a simple form

$$\#_u = |\#_\star - \#_o| \quad (4.5)$$

But with the identification of half of this as the net ground-state spin (each unpaired electron contributing a spin of 1/2 to the net spin), one recovers a rigorous theorematic[35] result for the nearest-neighbor (spin $^1/_2$) Heisenberg model, which in fact is equivalent to the Pauling−Wheland VB model on the full covalent space. In fact, this result for the ground-state spin also agrees with the exact theorematic result for the Hubbard model,[36] with full configuration interaction computations[37] on Hubbard−PPP for a fairly comprehensive list of structures up to around a dozen sites and with several high-quality configuration interaction ab initio computations (as mentioned in reviews 38 and 39). Indeed, for conjugated hydrocarbons the number of cases of experimental disagreement with this simple rule seem to be much fewer than the cases of agreement (also as mentioned in reviews 38 and 39). Therefore, this agreement lends support to our resonance theoretic arguments (which not only predict but also indicate to some degree the location of unpaired spins and in some cases the strength of spin pairings, which, if between distant sites, lead to low-lying excited states where these weakly paired sites are unpaired). Also, theorematic results for the sign of the spin density on the starred and unstarred sites are available[40] and are in qualitative agreement with the simple resonance theoretic model.

5. MO Theoretic Arguments

Quantitative MO theoretic arguments and computations are on the whole more conventionally made than are VB theoretic arguments and computations. There are different manners of establishing MO theoretic results, but in the treatment of edge localization effects the most common approach so far explored attempts to treat different translationally symmetric edges individually. In particular, polymer strips of arbitrary width w and with edges as in Figures 2a, 3a,b,d, and 4w have been previously treated,[12−16] and (along with further work here) a general pattern of behavior emerges. Basically, bands labeled with a one-dimensional wave vector k (corresponding to the translational symmetry along the polymer strip) arise and typically give orbitals that are smeared out not only along the length of the polymer strip but usually also across the strip.

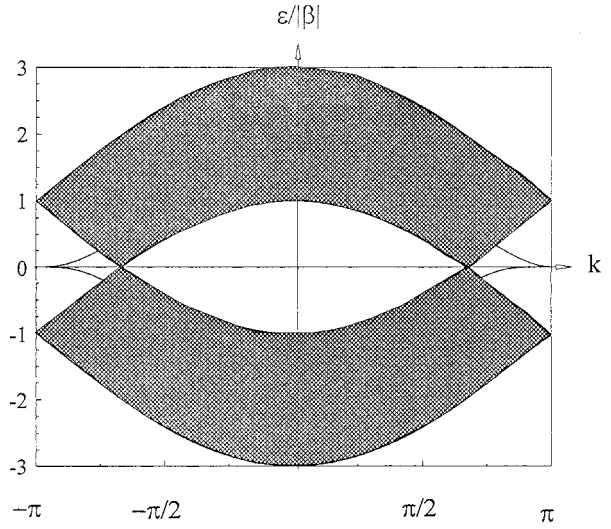

Figure 10. Overall pattern of band structure for arbitrary width strips with acenic (zigzag) edges. The bulk bands occupy the shaded region, and the exceptional edge-localized bands penetrate into the regions $-\pi \le k < -2\pi/3$ and $2\pi/3 < k \le \pi$, with the displayed bands being for the strips of widths $w = 1$, 2, 3, and 4.

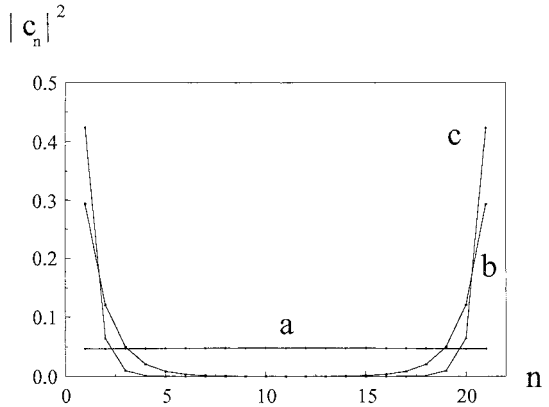

Figure 11. Frontier orbital densities as a function of distance from the edge of a width $w = 20$ graphitic strip with acenic edges. The probability $|c_n|^2$ represents (in the notation of Appendix C) the quantity $|(na|\epsilon)|^2 + |(nb|\epsilon)|^2$ associated with a transfer matrix "propagation cell" (which in the absence of the edge would devolve into a unit cell of graphite).

Still, occasionally there are portions of some bands that are exceptional; these *edge-localized* orbitals, though smeared out along the length of the polymer, fall off overall exponentially in amplitude with distance from the edges and are very nearly nonbonding (rapidly approaching nonbondedness exponentially with strip width). For instance, within the Hückel theoretic approximation for the polyacenic edges of Figure 3a the band energies $\varepsilon \equiv |\beta|\epsilon$ appear as indicated in Figure 10 with the bulk of the bands for any width w being confined to the shaded regions indicated there. Indeed, there is but a portion of a single bonding band (and a single corresponding antibonding band) that penetrates outside this shaded region, and it is that of the exceptional orbitals. This exceptional band portion is shown for the case of widths $w = 1$, $w = 2$, $w = 3$, and $w = 4$ in the first, second, third, and fourth quadrants of the ϵ vs k plot of the figure, where one sees that this exceptional band portion tends to close in on the nonbonding $\epsilon = 0$ Fermi level in the region where $2\pi/3 < |k| < \pi$ as the strip width w increases. Figure 11 shows the mean density (averaged over neighboring starred and unstarred sites) across a $w = 20$ strip for the bonding orbitals of exceptional type at $k = 0.75\pi$, 0.85π, and 0.95π, where one sees that the degree of edge localization is different at different k values; for the present type of edge, localization is stronger for larger $|k|$ values. The exceptional antibonding orbitals give much the same densities as the bonding orbitals, since these bonding and antibonding orbitals differ in amplitudes only in being symmetric or antisymmetric across the strip, where the node for the antisymmetric case occurs in the region where even for the symmetric orbital the amplitude is very small (in magnitude). Generally, symmetric/antisymmetric pairs of edge-localized band orbitals approach degeneracy as w increases, and if one is bonding while the other is antibonding, then the asymptotic degeneracy occurs at $\epsilon = 0$, as is discussed in Appendix C. Now any of the exceptional bonding and antibonding near-degenerate band orbitals (if combined to exhibit localization near just one edge) may be singly occupied with orbitals of different spins for different edges to yield a UHF wave function, which may be argued to be of lower energy than the (Hückel theoretic) RHF solution. That is, the cost of the UHF wave function to the Hückel part of the energy of an orbital of wave vector k is proportional to the corresponding band gap Δ_k, which comes ever closer to 0 for ever wider strips when dealing with the noted exceptional edge-localized orbitals; on the other hand, electron repulsion energy (proportional to the Hubbard parameter U) is in such cases saved, since the UHF orbitals on opposing edges are well separated with differential overlap between orbitals on opposite edges decreasing exponentially quickly as w increases. Thus, any such exceptional band orbitals give rise (in the UHF approximation for a Hubbard−PPP type model) to unpaired spin density near the edges.

But granted such an overall computational scheme for the recognition of edge-localized spin density, the question arises as to whether there might be any agreement with our simplified resonance theoretic predictions. Indeed, the net amount of such unpaired spin density along the different edges for the cases of Figures 2a and 3a,b and some other cases is found to be the same as predicted via the simple resonance theoretic argument. In fact, the density tends to be concentrated on just the same sites as predicted via the simple resonance theoretic argument. [After inclusion of the electron−electron interaction's effect in a UHF solution, the band gap is generally modified, as emphasized by Tyutyulkov et al,[19] and this is not considered here; the present point concerns its role in affecting the unpairing of spins.] In fact, some of the details noted for the polypolyacene case carry over to other cases, with some of the results best enunciated in terms of the edge symmetry classification idea involving the (x,y) labeling explained near eq 3.1. Generally, it seems that the ϵ vs k band diagram may be partitioned into two regions corresponding to whether there can occur edge-localized orbitals. And for edge symmetries $(x,y) = (1,0)$, these two regions are just as enunciated for the polypolyacene case of Figure 10, where the region without edge localization is shaded. That is, for $(x,y) = (1,0)$ it may be demonstrated as indicated in Appendix D that all edge nonlocalized orbitals are confined (for semi-infinite graphite) in the shaded region, which may be given analytically as bound by

$$\varepsilon = \pm\{2\cos(k/2) \pm 1\}\beta \qquad (5.1)$$

And any edge-localized orbitals that might occur would only arise in the unshaded region near the $\epsilon = 0$ Fermi level. Then for the limit of very wide strips any nonbonding bands penetrating into this unshaded region would cover sections of $^1/_3$ or $^2/_3$ (or all) of the full range of k-values, and just as for the resonance theoretic case, the consequent net number of unpaired

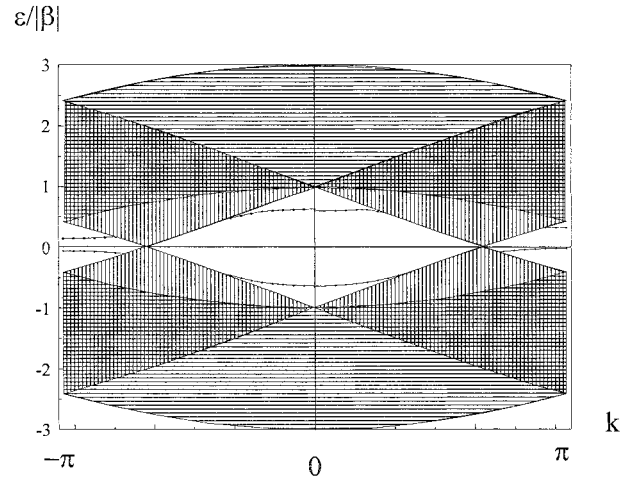

Figure 12. Overall pattern of band structure for arbitrary width strips with edges alternating between acenic (zigzag) and quinoidal structures, as in Figure 4h. The bulk bands occupy the shaded regions in the large-width limit, and the exceptional edge-localized bands penetrate into the regions $-\pi \le k < -2\pi/3$ and $2\pi/3 < k \le \pi$, with the displayed bands being for the strips of widths $w = 1$, 3, 5, and 7.

edge-localized electrons per unit cell would be an integer multiple of $^1/_3$. For $x \ge 2$ and $y = 0$ what apparently happens is that again there are two similar regions, with the shaded edge-nonlocalized region obtained from the corresponding $x = 1$ shaded region by first folding the plot so that all of the plot is precisely confined to a wave vector range with $|k| \le \pi/x$ and, second, rescaling k by a factor of x so that the wave vector range becomes $-\pi \le k \le +\pi$. Thus, for $x = 2$, folds are made at $k = \pm\pi/2$ and then the k-values doubled, where for the $(x,y) = (2,0)$ edge symmetry of Figure 4h a band diagram plot of Figure 12 results. There the bands penetrating into the edge-localized regions in the first, second, third, and fourth quadrants are for strips of widths $w = 1$, 3, 5, and 7, with the edge-localized bands converging more closely to $\epsilon = 0$ as the width increases. Here, part of the shaded region is shown as singly shaded and part as doubly shaded, in correspondence with how the singly shaded regions of $x = 1$ fold over one another in the construction for the shaded region for the $x = 2$ case. In the doubly shaded region one can anticipate that on the average the density of states is twice that as in the singly shaded regions (because the folding of the band diagram is just a means for enlarging the unit cell while correspondingly diminishing the Brillouin zone, though the bulk orbitals being dominated by the interior is not really changed, since the rationale for the enlargement of the unit cell is only manifest near the edges). In Figure 12 there are additional bands near $k = 0$ penetrating outside the shaded region though they are not so near $\epsilon = 0$; as w increases, these bands remain well away from $\epsilon = 0$ in the nonshadow region, and upon examination they are found to be edge-localized. But these additional edge-localized orbitals being bonding should (for the neutral hydrocarbons) be doubly occupied in UHF wave functions and so do not contribute to unpaired spin density. Related types of plots are shown in Figure 13 for the $(x,y) = (2,0)$ edges of Figure 4k,l, as occur on strips of large widths ($w = 20$); here, all the eigenvalues (for positive k) are shown at a selection of 25 equally spaced k-values from $k = 0$ to $k = \pi$, where now the densities of the bands in the earlier shaded regions can be directly perceived. But also shown in Figure 13 is a similar plot for a width $w = 23$ strip with $(x,y) = (2,1)$ edges of the type in Figure 4m and also for a width $w = 25$ strip with $(x,y) = (1,1)$ edges of Figure 4e. In all these cases for fairly wide strips the edge-localized orbitals have energies very close to nonbonding energies at $\epsilon = 0$ and are clearly manifested in these plots. Finally, in a general vein (for general (x,y) symmetry) the shadow regions always touch the nonbonding $\epsilon = 0$ position at $k = \pm\pi/3$ or $k = \pm 2\pi/3$ if $x - y$ is not divisible by 3, and at $k = 0$ otherwise, all is consistent with our band theoretic picture supporting the symmetry−integrality condition for unpaired electrons derived in the resonance theoretic picture. Incidentally, the number of unpaired electrons per unit cell of edge is then an integer multiple of 3. These general results are argued in Appendix E. Overall support for the simple resonance theoretic predictions is obtained.

Particularly, Fujita and co-workers[12−14] have made band theoretic computations on a number of different width strips with different edges of a few particular types. Their edge types included the zigzag $(x,y) = (1,0)$ edge as in Figure 3a, the arm-chair $(x,y) = (1,1)$ edge as in Figure 2a, and a few mixed zigzag/arm-chair edges as in Figure 4l,w. Generally, they found that for the investigated strips of increasing widths, edge-localized band orbitals are in correspondence with the expectations outlined in the two preceding paragraphs. For a finite-width strip any such edge-localized orbitals from just above and below the Fermi level should then pair to give a UHF solution with even greater localization and less electron repulsion. They emphasized the edge-nonlocalizing behavior of the arm-chair edge structure, as contrasted with the edge-localizing behavior of the zigzag edge structure, and described it as "remarkable" that in the mixed zigzag/arm-chair case the zigzag structures engendered localization despite the presence of the delocalizing arm-chair structures. But all this is fairly easy to understand from the resonance theoretic considerations, which, for the type of mixed case $(x,1)$ that they considered, readily lead to a prediction of $(x - 1)/3$ unpaired electrons per unit cell of edge. In the last column of Table 1 these and other band theoretic computations for various edges are identified by reference. Band theoretic work in the current article is designated by either "here" when there are explicit computations or by a parenthetic "(here)" when there are more complete analytic treatments for $y = 0$ (as in Appendices C and D along with the discussion concerning Brillouin zone folding). It is emphasized that all these band theoretic results, both particular and general, are in agreement with the simple resonance theoretic predictions for the limit of very wide strips. There are some other band theoretic computations[41] on polyacenic strips of general widths, but the results have not focused on analyzing the band orbitals to test for edge-localization discussed here, though as we emphasize, this is very important in characterizing their (reactivity and magnetic) properties.

There is further support for the simple resonance theoretic predictions in Stein and Brown's computations[17,18] on large finite fragments (of up to 2300 π-centers). They treat sequences of increasingly larger hexagonal symmetry fragments with different types of edges as in Figures 2a,b and 3a,c, and they find frontier orbitals with densities concentrated along the edges precisely in the cases (namely, those of Figure 3a,c) where the resonance theoretic argument predicts locally unpaired spin density. Moreover, their edge-localized orbitals are evidently those with energies most near $\epsilon = 0$, and they approach $\epsilon = 0$ much more rapidly than the cases without edge localization. Further, most of the density of the edge-localized fronteir orbitals seem to generally appear in the same atomic locations as indicated from the resonance theoretic arguments. They do not seem to have checked how many other orbitals beyond the frontier orbitals might be edge-localized, and perhaps accurate estimates would be confounded by the finite sizes of their fragments. Presumably,

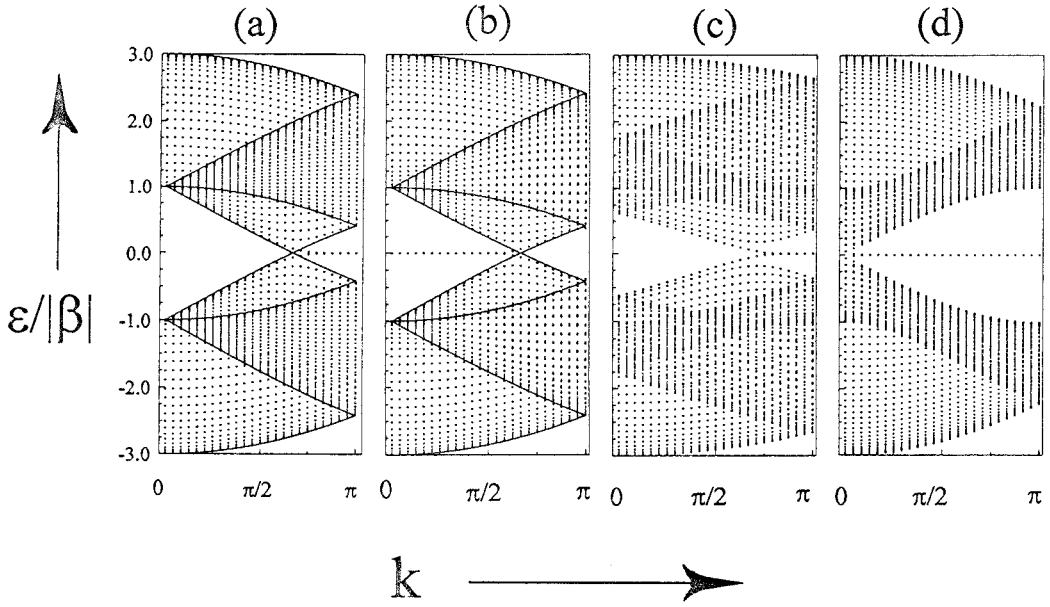

Figure 13. Band eigenspectra displayed at a selection of 25 *k*-values uniformly spaced from $k = 0$ to $k = \pi$. The structures for the four cases shown are (a) $w = 20$ with edges as in Figure 4k, (b) $w = 20$ as in Figure 4l, (c) $w = 23$ as in Figure 4m, and (d) $w = 25$ as in Figure 4e. In parts a and b the boundaries of the described "shaded regions" are drawn in.

TABLE 1: Edge Symmetries and Edge-Localized Unpaired Electrons per Unit Cell of Edge

structure in Figure 4	primitive translation (*x*,*y*)	unpaired electrons $\#_u$	band (or MO) theory refs
a	(1,0)	1/3	12, 13, (17, 18, 20), here
b	(1,0)	2/3	16, (here)
c	(1,0)	1/3	(here)
d	(1,1)	0	(17, 18), 15, 12, 13
e	(1,1)	1	here
f	(1,1)	0	
g	(1,1)	0	
h	(2,0)	1/3	here
i	(2,0)	2/3	(here)
j	(2,0)	2/3	(here)
k	(2,0)	1/3	(17, 18), here
l	(2,0)	2/3	here
m	(2,1)	1/3	14, here
n	(2,1)	2/3	
o	(2,1)	2/3	
p	(2,1)	4/3	
q	(2,1)	2/3	
r	(2,2)	0	
s	(2,2)	1	
t	(3,0)	0	(here)
u	(3,0)	0	(18), (here)
v	(3,0)	0	(here)
w	(3,1)	2/3	14

a UHF treatment from these orbitals would similarly yield unpaired spin density in the proper amounts along the edges, though this does not seem to have been carried out to the extent already done for the polymer strips of the preceding paragraph. The cases they have treated are also indicated in the last column of Table 1 with reference numbers enclosed in parentheses. Again, all that they do report is consistent with the simple resonance theoretic picture. Several other finite fragment computations by other researchers do not seem to have been analyzed for edge localization. But some[42] have concerned themselves with the rate at which the overall π-electron energy of increasingly larger clusters approach that of graphite, finding that precisely those that we identify as having edge-localized states show the slowest convergence (as we see should occur because it is precisely these structures that lead to an extra density of near-nonbonding occupied orbitals).

Further, there is some relevant theoretical evidence from early work by Dewar and Longuet-Higgins.[43] Their general results are neatly explained in terms of the *Pauling free valence*, which for a site *i* of a benzenoid G we define as the fraction of global Kekule structures that leave site *i* unpaired. Basically, for monoradical benzenoids Dewar and Longuet-Higgins establish a quantitative correspondence between such Pauling bond orders and Hückel MO orbital amplitudes for the nonbonding orbital. But these Pauling free valences are just a bit more sophisticated type of bond order than the implicit bond orders we have used, so this is further support for the general correspondence between MO and resonance theoretic results.

As a result of the various computations and the various partial proofs we have now noted, it is natural to speculate the following.

For the correspondence conjecture, let G be a semi-infinite bipartite graphitic carbon π-network with a translationally symmetric edge without any 4*n* rings. Then for the Hückel model of G, there are nonbonding edge-localized band orbitals whose number matches that of the unpaired electrons predicted from the simple resonance theoretic argument.

Indeed, there are even further natural speculations: about the exponential degree of edge localization, about the locations of the exceptional orbitals in the band diagram (outside the densely populated shaded region), about modifications appropriate for a finite-width strip, about the associated form of UHF solutions, and about the tendency for the locations of the associated unpaired spin density.

Finally, a few words may be said concerning the extension beyond simple Hückel MO theory. The extension to include electron−electron repulsion and associated exchange interaction is of course implicit in the consideration of UHF theory for Hubbard−PPP extended Hückel models, which we have already found is a necessary step in understanding the origin of unpaired electrons within the MO picture. But there are further approximations, say as concerns the restriction of electron-hopping integrals (β_{ij}) to constant values for nearest-neighbor sites only or as concerns the neglect of intersite overlap. Clearly, in the

interior of a wide strip the bond lengths should retain their bulk-favored uniform bond lengths, where the shadow regions for the bulk orbitals should remain the same. Near the edges different π-bond orders may of course be different, thereby giving different bond lengths, which in turn enhance π-bond localization and the validity of the classically interpretable VB theoretic picture. Another type of modification would be in terms of an "extended Hückel" model with intersite overlaps and nonneighbor electron-hopping integrals, and this is considered in Appendix E where we find that much of the simple Hückel based argument is only slightly altered.

6. Conclusion and Prospects

Simple structural rules governing the occurrence of free valences (or of locally unpaired spins) on graphitic edges have been developed. These rules are somewhat intuitively derived (from chemically appealing resonance theoretic ideas) in section 2, and the rules are enunciated in section 3 in conjunction with Figures 1−3. Numerous particular predictions are made in Table 1 (along with the associated Figure 4) in section 3, and some general predictions are made in a theorem. It is noted that the rules find general support: first, from the initially noted simple (yet presumably correct) resonance theoretic arguments (of section 2); second, from more elaborated resonance theoretic VB arguments (of section 4); third, in studied cases (especially with translationally symmetric edges) from MO or band theoretic arguments (as in section 5).

The commonality of MO and VB theoretic predictions for the same structures indicates a robustness for these particular predictions because of the quite different presumptions going into the MO and VB models. Thus, apparently the rules and particular predictions (given in section 3) seem to hold exceptional promise for guidance as to the character of different possible edges conceivable for graphitic fragments. Presumably, the edges with higher concentrations of edge-localized unpaired electrons would be reactive (as polyradicals) and under many preparatory conditions undergo additional reactions to quench this free valence. Notably because of the "symmetry−integrality" theorem of section 3, if an edge of translationally symmetry (x,y) is such that $x - y$ is not divisible by 3, then such reactions at the edge, to decorate it with a nonradical structure, would take place in such a way that the translational period is tripled (so that the new x and y being triples of the old would have $x - y$ divisable by 3). The ideas here incidently rationalize a number of earlier particular observations,[12−14,17−20,31−33,41,42] which were deemed unusual at the time but are evidently due to our (readily predicted) correlations between edge structure and edge-localized orbitals.

In addition to the influence of edge-localized orbital on chemical reactivity and magnetic properties, one might generally inquire about influences on electrical conductivity. But in this case elaborate (e.g., ab initio) computations seem to be required. Though at the Hückel level the edge-localized orbitals are precisely at the crucial Fermi level, we have emphasized that they split apart in a UHF solution of a Hubbard−PPP model. But the considerations are not complete because the bulk orbitals have low density at $\epsilon = 0$, and in fact, also the gap evidently opens slightly[44] for multilayer graphite. But also in extended Hückel theory one may expect the edge-localized orbitals to lower slightly in energy (as discussed in Appendix F) so that the upward split edge-localized orbitals may conceivably end up being quite close to the Fermi level and thereby affect the conductivity. Here, the delicacy of the effects makes an ab initio treatment desirable.

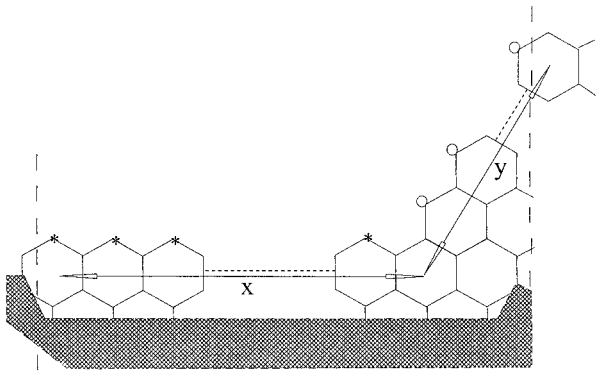

Figure 14. Special type of reference (x,y) edge.

It might be noted that some aspects of our resonance theoretic arguments carry much beyond the current focus on translationally symmetric graphite edges. Some ideas should carry over quite straightforwardly to deal with graphite with local defects, either at the edge or internally. But more generally, some of the ideas of section 3 hold for quite general bipartite conjugated networks. Even the simple resonance theoretic ideas should be treated more tentatively for the case of bipartite systems with four cycles (i.e., they should be viewed as subject to qualification or modification) because interaction around conjugated $4n$ circuits is not stabilizing (as is the essence of Hückel rule). Still, there is notable interest in resonance theoretic models for quite different systems, e.g., those involving the square-planar lattice for the understanding of high-temperature superconduction[45] and also Pauling's theory of metals.[46] Hopefully, the ideas developed here might still prove to be useful in other such areas.

Acknowledgment. Acknowledgment is made for discussions with many colleagues and for support from the Welch Foundation of Houston, Texas.

Appendix A: Proof of Symmetry−Integrality Theorem

First, for symmetry class (x,y), consider a special edge as in Figure 14. For this special case there are no degree 1 sites, so eq 3.2 reduces to $\#_u = |\#_{\bigstar 2} - \#_{\bigcirc 2}|/3$, and as seen from Figure 14, the degree-2 apex sites along the x-direction are of one type (chosen as ★ in the figure) while the degree-2 apex sites along the y-direction are of the other type (here ○ in the figure). Further noting that the numbers of these two types of sites are respectively x and y, one sees that $\#_u = (x - y)/3$, and the claim of the theorem is established for this particular type of edge.

Next, it is to be shown that however the unit cell of edge of a given (x,y) is modified, by adding (or subtracting) new sites from the special case of Figure 14, it turns out that $\#_u$ is modified from the reference value $\pm(x - y)/3$ by an integer, so (if this can be shown) the integerness (or nonintegerness) of $\#_u$ is conserved. Consider adding edges one at a time, where two patterns of connection to already preexisting sites are possible depending on whether the new site is attached to 1 or 2 of the earlier sites. Labeling the new site added by * and the site(s) to which it is attached by ○, one obtains the two connection patterns of Figure 15. For the single attachment case if the * is starred, then this attachment process adds a (zero-order) spin density of $+^2/_3$ at site * while the (zero-order) spin density at the attachment site ○ is decreased by $-^1/_3$ (from $-^2/_3$ to $-^1/_3$ or else from $-^1/_3$ to 0), so the net change in spin density is $+1$. If * is instead unstarred, then the net change in spin density is -1. For the case of Figure 15 the double-attachment process likewise yields a net change in spin density of ± 1. Thus, for

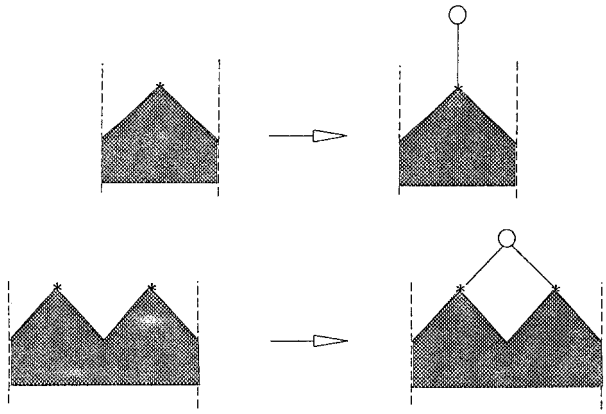

Figure 15. Processes for single and double attachments of one new site ○ to one or two preexisting sites labeled *.

each modification adding a single site, the integerness is conserved. And yet, it must be conserved on subtraction of sites (since starting with the site depleted, edge addition of sites conserves integerness). Thus, the theorem is proved.

Appendix B: Proof of the Pairing−Conservation Theorem

To establish the pairing conservation theorem of section 4, we presume a cut C to which are associated $C_\star$ and $C_\circ$. For a given Kekule structure K there is a value $\Delta(C,K)$ for the difference between the number of edges of K in $C_\star$ and $C_\circ$, and we let $S_\star(C,K)$ and $S_\circ(C,K)$ denote the respective numbers of starred and unstarred sites on the A-side of C such that all the sites of these $S_\star(C,K)$ are bonded to other sites in A. Of course, some of the sites in A may be bonded to sites on the other side B, and the numbers of such starred and unstarred sites evidently are $|K\cap C_\star|$ and $|K\cap C_\circ|$. Thus, the total numbers $\#_\star(C)$ and $\#_\circ(C)$ of starred and unstarred sites on the A-side of the cut C may be decomposed as

$$\#_\star(C) = |S_\star(C,K)| + |K\cap C_\star| \quad \text{and}$$
$$\#_\circ(C) = |S_\circ(C,K)| + |K\cap C_\circ|$$

Then from this and the fact that for K the numbers of starred and unstarred sites bonded within A must be equal (for a bipartite graph), it follows that

$$\#_\star(C) - \#_\circ(C) = \{|S_\star(C,K)| + |K\cap C_\star|\} - \{|S_\circ(C,K)| + |K\cap C_\circ|\} = \pm\Delta(C,K)$$

Since the left-hand side of this equation is independent of K, so must be the right-hand side, and the proof is complete.

Appendix C: Edge Localization, Asymptotic Degeneracy, and Nonbondedness

First, for semi-infinite graphite, let us suppose an energy ϵ edge-localized eigenorbital ψ, with amplitudes decaying rapidly into the interior. Identify a sequence of bonds at a given large distance d from the edge such that this sequence exhibits the same translational symmetry as the edge. Then presuming that these bonds when cut end up disconnecting the edge from the interior at distances greater than d, imagine a reflected duplicate of this strip and form a strip of width $2d$ by joining these two halves together. Since the considered orbital ψ has decayed to a very small amplitude at the (large) distance d, one can expect symmetric and antisymmetric combinations $\psi + \sigma\psi \equiv \psi_+$ and $\psi - \sigma\psi \equiv \psi_-$ to be (essentially) the eigenorbitals of the strip.

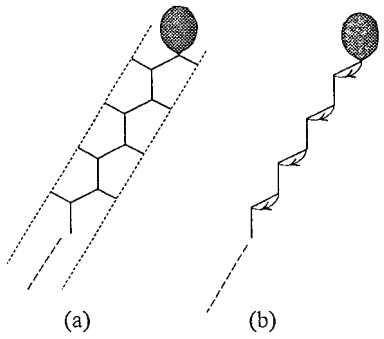

Figure 16. Unit cell for $(x,y) = (1,0)$ is shown in part a, and in part b for the solution of the Hückel model there appears the associated quasi-one-dimensional graph (with k-dependent weights $e^{\pm ik_x}$ on the directed edges).

Evidently, these new eigenorbitals are energetically split but very slightly from ϵ, and this splitting will rapidly approach 0 as the width is increased. These asymptotically degenerate orbitals then make the orbitals ψ and $\sigma\psi$ that are localized on opposite edges good candidates for UHF eigenorbitals if the splitting makes ψ_+ and ψ_- bonding and antibonding. Further, the strip construction implies that the reflection σ interchanges starred and unstarred sites. Then in $\sigma\psi$ and ψ as well as in ψ_+ and ψ_- the roles of starred and unstarred sites are interchanged. Hence, often ψ_+ and ψ_- are just the paired orbitals of Coulson and Rushbrooke,[23] where they have energies oppositely displaced from 0. In such a case with asymptotic degeneracy, they are both close to $\epsilon = 0$ and asymptotically nonbonding.

One may conversely presume a length of band of essentially nonbonding eigenorbitals. Though the band gap (or HOMO−LUMO) for graphite is 0, it is known that the bulk density of states drops to 0 at this energy. Thus, the orbitals corresponding to such a band portion should generally not be bulk orbitals, where they are edge-localized.

Appendix D: Band Characteristics for $(x,y) = (1,0)$ Edges

It is wished to establish the band diagram locations of edge-nonlocalized and edge-localized band orbitals when the edges are associated with a symmetry with $(x,y) = (1,0)$. In this case the unit cell is just one hexagon in width and may be chosen to be of the shape indicated in Figure 16a. Then the Hückel eigenvalue problem in k-space takes (see, for example, ref 47) the form of a graph theoretic adjacency matrix eigenvalue problem with a weighted adjacency matrix for a weighted graph as indicated in Figure 16b, where the solid edges are of weights β and the dashed edges are of weights $\beta\, e^{\pm ik}$, with the + or − sign applied here as the element corresponds or anticorresponds to the edge direction. Evidently, this matrix appears much like that for a linear chainlike problem, with a period of repetition every two sites, so that the sites might be numbered as indicated in Figure 16b. Then letting $|\epsilon)$ denote the Hückel eigenvector with a p,cth component $(p,c|\epsilon)$, the eigenequation may be expressed in the form

$$\beta_+(p,b|\epsilon) + \beta(p+1,b|\epsilon) = \varepsilon(p,a|\epsilon)$$
$$\beta(p,a|\epsilon) + \beta_-(p+1,b|\epsilon) = \varepsilon(p,b|\epsilon) \qquad \text{(D.1)}$$

where $\beta_\pm \equiv \beta(1 + e^{\pm ik})$ and the integer index p is large enough to represent a position away from the edge. Following a general "transfer matrix" technique that has proved to be useful for open chains[48] and with boundary states,[49,50] eq D.1 can be rewritten as

$$\begin{bmatrix} -\varepsilon & \beta_+ \\ \beta & 0 \end{bmatrix}\begin{pmatrix}(p,a|\epsilon)\\(p,b|\epsilon)\end{pmatrix}=\begin{pmatrix}0 & -\beta \\ -\beta_- & \varepsilon\end{pmatrix}\begin{pmatrix}(p+1,a|\epsilon)\\(p+1,b|\epsilon)\end{pmatrix} \quad \text{(D.2)}$$

Or if the left-hand-side matrix is inverted, then it appears as

$$\begin{pmatrix}(p+1,a|\epsilon)\\(p+1,b|\epsilon)\end{pmatrix}=\frac{1}{\beta\beta_-}\begin{pmatrix}\varepsilon^2-\beta^2 & -\varepsilon\beta_+ \\ \varepsilon\beta_- & -\beta_-\beta_+\end{pmatrix}\begin{pmatrix}(p,a|\epsilon)\\(p,b|\epsilon)\end{pmatrix} \quad \text{(D.3)}$$

Here, there appears on the right-hand-side a 2×2 *transfer* matrix **T**, which carries the eigenfunction amplitudes at position p to the eigenfunction amplitudes at position $p + 1$. And evidently, these amplitudes will propagate without diminution or growth (i.e., lead to a bulk smeared out orbital) if and only if the eigenvalues to **T** are of unit magnitude. Now these eigenvalues to **T** are

$$x_\pm = (2c)^{-1}\{\epsilon^2 - 1 - c^2 \pm [(\epsilon^2 - 1 - c^2)^2 - 4c^2]^{1/2}\}\, e^{ik/2} \quad \text{(D.4)}$$

where abbreviations $\epsilon \equiv \varepsilon/|\beta|$ and $c \equiv 2\cos(k/2)$ have been used. Now if the discriminant is negative, then

$$|x_\pm| = (2c)^{-1}\{(\epsilon^2 - 1 - c^2)^2 + [4c^2 - (\epsilon^2 - 1 - c^2)^2]\}^{1/2} = 1 \quad \text{(D.5)}$$

so the associated orbital has components that penetrate without diminution of magnitude into the interior. Thus, the condition for edge nonlocalization of an orbital is that the discriminant in eqs D.4 and D.5 be nonpositive:

$$(\epsilon^2 - 1 - c^2)^2 - 4c^2 \le 0 \quad \text{(D.6)}$$

Or with factorization and a focus on strict inequality, this becomes

$$(\epsilon - 1 - c)(\epsilon + 1 + c)(\epsilon - 1 + c)(\epsilon + 1 - c) < 0 \quad \text{(D.7)}$$

(where the special case of equality leads to Bizco's "intermediate" orbitals[50]). Then to satisfy eq D.7, either one or three of the factors on the left-hand side of this equation are to be negative, and it follows that the nonlocalized band orbitals have energies confined to the shaded areas of Figure 12, with the shaded areas having boundaries given by eq 5.1.

Appendix E: *k*-Space Location of Nonbonding Shadow Region

The shadow region is determined by the delocalized or bulk orbitals, which are on the whole like those in extended graphite. Thus, the shadow region in the Brillouin zone should be determined from the solutions for extended graphite, for which there are two independent translational symmetries, which we take to be in the *x*- and *y*-directions identified in the characterization of edge symmetries, near eq 3.1. Then the graphitic Hückel model reduces to the solution of a 2×2 matrix with wave-vector-dependent elements. This matrix can be viewed as equivalent to that for the adjacency matrix for a weighted graph, as in Figure 17, with the *x*- and *y*-directed edges with weights $\beta\, e^{\pm ik_x}$ and $\beta\, e^{\pm ik_y}$. Therefore, this matrix has diagonal elements of 0 and one off-diagonal element $\beta\{1 + e^{ik_x} + e^{ik_y}\}$, while the other is the complex conjugate of this. Thus, the orbital eigenvalues for extended graphite are

$$\varepsilon = \pm\beta|1 + e^{ik_x} + e^{ik_y}| \quad \text{(E.1)}$$

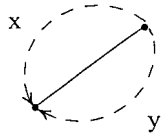

Figure 17. Band theory graph for the graphite unit cell.

For edges of symmetry (x,y) the basic translation defining the edge-attentive unit cells involves x steps in the x-direction and y steps in the y-direction, so the wave vector associated with such a translation is

$$k \equiv xk_x + yk_y \quad \text{(E.2)}$$

and the bulk graphitic energies expressed in terms of this are

$$\epsilon = \pm\beta|1 + \exp[i(k - yk_y)/x] + \exp(ik_y)| \quad \text{(E.3)}$$

The shadow region then is at a given k by the envelope of this function as k_y varies between $-\pi$ and $+\pi$. And of special interest is where the shadow region touches the (nonbonding) Fermi level at $\epsilon = 0$. From eq E.1 it is evident that the graphitic bands touch $\epsilon = 0$ only at two wave vector values, namely, $(k_x,k_y) = \pm(2\pi/3,-2\pi/3)$, which then corresponds to a edge-attentive wave vector of

$$k = \pm 2\pi(x - y)/3 \quad \text{(E.4)}$$

which of course we take modulo 2π (to fit it into the first Brillouin zone). That is, there are just three manners in which the shadow region touches $\epsilon = 0$, namely, at

$$k = 0, \quad \text{if } x - y \text{ is an integer multiple of 3}$$
$$k = \pm\pi/3, \quad \text{if } |x - y| \text{ is 1 more than an integer multiple of 3}$$
$$k = \pm 2\pi/3, \quad \text{if } |x - y| \text{ is 1 less than an integer multiple of 3} \quad \text{(E.5)}$$

Further, because from Appendix C the edge-localized orbitals must, for the Hückel model for semi-infinite graphite, be nonbonding, any edge-localized band would proceed (at $\epsilon = 0$) between the k locations of eq E.5 allowed for the particular (x,y) involved. That is, for example, for the last case of eq E.5, any edge-localized band would cover the k-space regions either with $2\pi/3 < |k| < 2\pi$ or with $0 < |k| < 2\pi/3$. Thus, the number of unpaired (edge-localized) electrons per edge-attentive unit cell is necessarily a multiple of $^1/_3$, and if $x - y$ is divisible by 3, it must be an integer.

Appendix F: Extended Hückel Theory

The simplest version of extended Hückel theory[51] entails inclusion of overlaps s to nearest neighbors and of next-neighbor electron-hopping integrals β'. Let **A** be the (nearest-neighbor) adjacency matrix so that the ordinary Hückel matrix is $\mathbf{H} = \alpha\mathbf{I} + \beta\mathbf{A}$, though often one takes $\alpha = 0$, since this only shifts the one-electron eigenspectrum (though retaining a nonzero value would be important in dealing with ionization energies). Similarly, let **A′** denote the matrix of next-nearest-neighbor "adjacencies" so that the slightly extended Hückel model we consider has Hamiltonian and overlap matrices

$$\mathbf{H}' = \alpha\mathbf{S} + \beta\mathbf{A} + \beta'\,\mathbf{A}' \quad \text{and} \quad \mathbf{S} = \mathbf{I} + s\mathbf{A} \quad \text{(F.1)}$$

One may verify that if we let $\mathbf{\Delta}$ denote the diagonal matrix of site degrees, then

$$\mathbf{A}' = \mathbf{A}^2 - \mathbf{\Delta} \qquad \text{(F.2)}$$

But except for the edges, $\mathbf{\Delta}$ is the same as $3\mathbf{I}$, so for bulk properties $3\mathbf{I} - \mathbf{\Delta}$ is a negligible perturbation. That is, for bulk properties (i.e., properties independent of details of the edge) a very close approximation results if we use

$$\mathbf{H}^0 = \alpha\mathbf{S} + \beta\mathbf{A} + \beta'(\mathbf{A}^2 - 3\mathbf{I}) \quad \text{and} \quad \mathbf{S} = \mathbf{I} + s\mathbf{A} \qquad \text{(F.3)}$$

Then $\mathbf{A}$, $\mathbf{H}$, $\mathbf{H}^0$, and $\mathbf{S}$ all have common eigenvectors, and if λ denotes an eigenvalue of $\mathbf{A}$, the corresponding eigenvalue for the generalized eigenvalue associated with $\mathbf{H}^0$ and $\mathbf{S}$ is

$$\epsilon^0 = \alpha + \{\beta\lambda + \beta'(\lambda^2 - 3)\}/(1 + s\lambda) \qquad \text{(F.4)}$$

Or when the eigenspectrum is shifted so that $\alpha = 3\beta'$, then

$$\epsilon^0 = \lambda\{\beta + \beta'(\lambda + 3s)\}/(1 + s\lambda) \qquad \text{(F.5)}$$

where one sees that for sufficiently (and typically) small s and β' the orbitals (and their energies) retain their identity as bonding, nonbonding, and antibonding. That is, so far as the bulk orbital energies are concerned, there is just a ϵ-dependent rescaling, and in particular, the shaded regions of our band diagrams appear "essentially" as before, being distorted in shape but touching the nonbonding $\epsilon = 0$ Fermi level at precisely the same k values. The exceptional bands that penetrate out of the shaded regions of the band diagram involve edge localization so that the edge-localized perturbation $\beta'(3\mathbf{I} - \mathbf{\Delta})$ might be considered. Indeed, this perturbation is an attraction to the edge regions, so it only enhances the edge localization and diminishes the subsequent Hückel gap between their symmetric and antisymmetric forms. Therefore, the cost for their UHF mixing is again negligible, so the UHF solution still applies and gives rise to the same amount of unpaired spin density localized near the edges.

References and Notes

(1) Bradburn, M.; Coulson, C. A.; Rushbrooke, G. S. *Proc. R. Soc. Edinburgh A* **1948**, *62*, 336. Coulson, C. A.; Rushbrooke, G. S. *Proc. R. Soc. Edinburgh A* **1948**, *62*, 350.

(2) Wallace, P. R. *Phys. Rev.* **1947**, *71*, 622.

(3) Hite, G. E.; Metropoulos, A.; Klein, D. J.; Schmalz, T. G.; Seitz, W. A. *Theor. Chim. Acta* **1986**, *69*, 369.

(4) For a focus on this area from a somewhat chemical view, see the following. Klein, D. J.; Zhu, H.-Y.; Valenti, R.; Garcia-Bach, M. A. *Int. J. Quantum Chem.* **1997**, *65*, 421. But too the great body of work in the physics literature becoming of such great interest (in connection with high-temperature superconductivity) during the past dozen years is reviewed from a rather different perspective in the following. Manousakis, E. *Rev. Mod. Phys.* **1991**, *63*, 1. Barnes, T. *Int. J. Mod. Phys. C* **1991**, *2*, 659. Senatore, G.; March, N. H. *Rev. Mod. Phys.* **1994**, *66*, 445. Dagotto, E. *Rev. Mod. Phys.* **1994**, *66*, 763.

(5) See, for example, the following. Iijima, S. *Nature* **1991**, *354*, 56. Smalley, R. E. *Materials Sci. Eng. B* **1993**, *19*, 1. Arayan, P. M. Iijima, S. *Nature* **1993**, *361*, 33. Ebbesen, T. W. *Phys. Today* **1996**, 26. Hsu, W. K.; Terrones, M.; Hare, J. P.; Terrones, H.; Kroto, H. W.; Walton, D. R. M. *Chem. Phys. Lett.* **1996**, *262*, 161. Endo, M., Iijima, S., Dresselhaus, M. S., Eds. *Carbon Nanotubes*; Pergamon: New York, 1996. Yakobson, B. I.; Smalley, R. E. *Am. Sci.* **1997**, *85*, 324.

(6) Donnet, J. B.; *Carbon* **1982**, *20*, 267. Lewis, I. C. *Carbon* **1982**, *20*, 519. Wigmans, T.; Hoogland, A.; Tromp, P.; Moulijn, J. A. *Carbon* **1983**, *21*, 113. Ayache, J.; Oberlin, A.; Inagaki, M. *Carbon* **1990**, *28*, 337. Mose-Yacaman, M.; Terrones, H.; Rendon, L.; Dominguez, J. M. *Carbon* **1995**, *33*, 669.

(7) McClure, J. M.; Hickman, B. B. *Carbon* **1982**, *20*, 373. Ishii, C.; Shindo, N.; Kaneko, K. *Chem. Phys. Lett.* **1995**, *242*, 196. Ishii, C.; Matsumura, Y.; Kaneko, K. *J. Phys. Chem.* **1995**, *99*, 5743.

(8) Pauling, L. *The Nature of the Chemical Bond*; Cornell University Press: Ithaca, New York, 1939.

(9) Seitz, W. A.; Klein, D. J.; Schmalz, T. G.; García-Bach, M. A. *Chem. Phys. Lett.* **1986**, *115*, 139.

(10) Davison, S.; Steślicka, M. *Basic Theory of Surface States*; Clarendon Press: Oxford, 1992.

(11) Hoffmann, R. *Rev. Mod. Phys.* **1998**, *60*, 601.

(12) Fujita, M.; Wakabayashi, K.; Nakada, K.; Kusakabe, K. *J. Phys. Soc. Jpn.* **1996**, *65*, 1920. Wakabayashi, K.; Fujita, M.; Kusakabe, K.; Nakada, K. *Czech. J. Phys.* **1996**, *46*, 1865.

(13) Nakada, K.; Fujita, M.; Wakabayashi, K.; Kusakabe, K. *Czech. J. Phys.* **1996**, *46*, 2429.

(14) Nakada, M.; Fujita, M.; Dresselhaus, G.; Dresselhaus, M. S. *Phys. Rev. B* **1996**, *54*, 17954.

(15) Klein, D. J. *Rep. Mol. Theory* **1990**, *1*, 91.

(16) Klein, D. J. *Chem. Phys. Lett.* **1994**, *217*, 261.

(17) Stein, S. E.; Brown, R. L. *Carbon* **1985**, *23*, 105. Stein, S. E.; Brown, R. L. *J. Am. Chem. Soc.* **1987**, *109*, 3721.

(18) Stein, S. E.; Brown, R. L. In *Molecular Structure and Energetics*; Liebman, J., Greenberg, A., Eds.; VCH: New York, 1987; Vol. 2, pp 37−66.

(19) Tyutyulkov, N. N.; Madjarova, G.; Dietz, F.; Müllen, K. *J. Phys. Chem. B* **1998**, *102*, 10183.

(20) Bulusheva, L. G.; Okotrub, A. V.; Romanov, D. A.; Tomanek, D. *Phys. Low-Dimens. Semicond. Struct.* **1998**, *3/4*, 107.

(21) See many organic chemistry texts and especially the following. Wheland, G. W. *Resonance in Organic Chemistry*; John Wiley & Sons: New York, 1955. Clar, E. *Polycyclic Hydrocarbons, I & II*; Academic Press: New York, 1964.

(22) This is discussed in parts 7−5 and 7−6 of the 1960 third edition of ref 8, and also see the following. Ham, N. S.; Ruedenberg, K. *J. Chem. Phys.* **1959**, *29*, 1215.

(23) See ref 11 or many theoretical organic chemistry texts and following original reference. Coulson, C. A.; Rushbrooke, G. S. *Proc. Cambridge Philos. Soc.* **1940**, *36*, 193.

(24) See ref 9 or the following. Pauling, L. *J. Chem. Phys.* **1933**, *1*, 280. Pauling, L.; Wheland, G. W. *J. Chem. Phys.* **1933**, *1*, 362. Simonetti, M.; Gianinetti, E.; Vandoni, I. *J. Chem. Phys.* **1968**, *48*, 1579.

(25) For a general review see the following. Chein, J. C. W. *Polyacetylene*; Academic Press: New York, 1984.

(26) See, for example, the following. Chance, R. R.; Boudreaux, D. S.; Eckhardt, H.; Elsenbaumer, R. L.; Frommer, J. E.; Bredas, J. L.; Silbey, R. In *Quantum Chemistry of Polymers—Solid State Aspects*; Ladik, J., et al.; Eds.; D. Reidel Publishing Co.: Dordrecht, 1984; pp 221−248. Soos, Z. G.; Etemad, S.; Galvao, D. S.; Ramasesha, S. *Chem. Phys. Lett.* **1992**, *194*, 341. Cuff, L.; Kertesz, M. *Macromolecules* **1994**, *27*, 762.

(27) Klein, D. J.; Hite, G. E.; Seitz, W. A.; Schmalz, T. G. *Theor. Chim Acta* **1986**, *69*, 409. Klein, D. J.; Schmalz, T. G.;. Seitz, W. A.; Hite, G. E. *Int. J. Quantum Chem.* **1986**, *19*, 707.

(28) See, for example, the following. Cyvin, S. J.; Gutman, I. *Kekule Structures in Benzenoid Hydrocarbons*; Springer-Verlag: Berlin. 1988 and most of the references therein.

(29) Klein, D. J.; Zivković, T. P.; Valenti, R. *Phys. Rev. B* **1991**, *43*, 723.

(30) Herndon, W. C. *Thermochim. Acta* **1974**, *8*, 225. Randić, M. *J. Am. Chem. Soc.* **1977**, *99*, 444.

(31) Yen, T. F. *Theor. Chim. Acta* **1971**, *20*, 399.

(32) Gordon, M.; Davison, W. H. T. *J. Chem. Phys.* **1952**, *20*, 428.

(33) Elser, V. *J. Phys. A* **1984**, *17*, 1509.

(34) Hurst, C. A.; Green, H. S. *J. Chem. Phys.* **1960**, *33*, 1059. Kasteleyn, P. W. *J. Math. Phys.* **1963**, *4*, 287. Fisher, M. E. *Rev. Mod. Phys.* **1974**, *46*, 597.

(35) Lieb, E. H.; Mattis, D. C. *J. Math. Phys.* **1962**, *3*, 749. Klein, D. J.; Nelin, C. J.; Alexander, S. A.; Matsen, F. A. *J. Chem. Phys.* **1982**, *77*, 3101.

(36) Lieb, E. H. *Phys. Rev. Lett.* **1989**, *62*, 1201.

(37) Klein, D. J.; Alexander, S. A.; Randić, M. *Mol. Cryst. Liq. Cryst.* **1989**, *176*, 109.

(38) See, for example, articles in the following. *Diradicals*; Borden, W. T., Ed.; John Wiley & Sons: New York, 1982.

(39) See, for example, articles in the following. *Magnetic Properties of Organic Materials*; Lahti, P. M., Ed.; Marcel Dekker: New York, 1999.

(40) Cheranovski, V. O. *Teor. Eksp. Khim.* **1980**, *16*, 147. Klein, D. J.; Alexander, S. A. In *Graph Theory and Topology in Chemistry*; King, R. B., Rouvray, D. H., Eds.; Elsevier: Amsterdam, 1987; pp 404−419.

(41) Misurkin, I. A.; Ovchinnikov, A. A. *Teor. Eksp. Khim.* **1968**, *4*, 3. Yamabe, T.; Tanaka, K.; Ohzeki, K. *Solid State Commun.* **1982**, *44*, 823. Kertesz, M.; Hoffmann, R. *Solid State Commun.* **1983**, *47*, 97. Mehandru, S. P.; Anderson, A. B.; Angus, J. C. *J. Phys. Chem.* **1992**, *96*, 10978.

(42) Hosoya, H.; Kumazaki, H.; Chida, K.; Ohuchi, M.; Gao, Y.-D. *Pure Appl. Chem.* **1990**, 62, 445. Hosoya, H.; Tsukano, Y.; Ohuchi, M.; Nakada, K. *Nat. Sci. Rep. Ochanomizu Univ.* **1993**, *44*, 155. Randić, M.; Tsukano, Y.; Hosoya, H. *Nat. Sci. Rep. Ochanomizu Univ.* **1994**, *45*, 101.

(43) Dewar, M. J. S.; Longuet-Higgins, H. C. *Proc. R. Soc. A* **1952**, *214*, 482.

(44) Slonczewski, J. C.; Weiss, P. R. *Phys. Rev.* **1958**, *109*, 272. Charlier, J.-C.; Michenaud, J.-P.; Gonze, X.; Vigneron, J.-P. *Phys. Rev. B* **1991**, *44*, 13237.

(45) Rokhsar, D. S.; Kivelson, S. A. *Phys. Rev. Lett.* **1988**, *61*, 2376. Kivelson, S. A. *Phys. Rev. B* **1989**, *39*, 259.

(46) Pauling, L. *J. Solid State Chem.* **1984**, *54*, 297. Kamb, B.; Pauling, L. *Proc. Natl. Acad. Sci. U.S.A.* **1985**, *82*, 8284. Pauling, L.; Kamb, B. *Proc. Natl. Acad. Sci. U.S.A.* **1986**, *83*, 3569.

(47) Tang, A.-C.; Kiang, Y.-S.; Yan, G.-S.; Tai, S.-S. *Graph theoretical molecular orbitals*; Science Press: Beijing, 1986.

(48) Hoffmann, T. A.; Kónya, A. *J. Chem. Phys.* **1948**, *16*, 1172. Hoffmann, T. A. *J. Chem. Phys.* **1950**, *18*, 989. Kerner, E. H. *Phys. Rev.* **1954**, *95*, 687. Hori, J.; Asahi, H. *Prog. Theor. Phys.* **1957**, *17*, 425. Matsuda, H. *Prog. Theor. Phys.* **1962**, *23*, 22. Asahi, T. *Prog. Theor. Phys.* **1962**, *23*, 59.

(49) Fromm, O.; Koutecky, J. In *Catalysis in Chemistry and Biochemistry*: *Theory and Experiment*; Pullman, B. D., Ed.; Reidel: New York, 1979. Lee, D. H.; Joannopoulos, J. D. *Phys. Rev. B* **1981**, *23*, 4988, 4997. Bizcó, G.; Fromm, O.; Koutecky, O. J.; Lee, A. *Chem. Phys.* **1985**, *98*, 51. Gies, M.; Seel, M.; Ladik, J. *J. Mol. Struct.* **1987**, *150*, 267.

(50) Bizcó, G. *Ned. Tijdschr. Vacuumtech.* **1978**, *16*, 195. Bizcó, G.; Lukovits, I. *Int. J. Quantum Chem.* **1979**, *16*, 31. Bizcó, G. *Stud. Biophys.* **1983**, *93*, 241.

(51) Hoffmann, R. *J. Chem. Phys.* **1963**, *39*, 1397.